Matter waves of Bose-Fermi mixtures in one-dimensional optical lattices

Yu. V. Bludov,[1,*] J. Santhanam,[2,†] V. M. Kenkre,[2,‡] and V. V. Konotop[1,3,§]

[1]*Centro de Física Teórica e Computacional, Universidade de Lisboa, Complexo Interdisciplinar,*
Avenida Professor Gama Pinto 2, Lisboa 1649-003, Portugal

[2]*Consortium of the Americas for Interdisciplinary Science and Department of Physics and Astronomy, University of New Mexico,*
Albuquerque, New Mexico 87131, USA

[3]*Departamento de Física, Universidade de Lisboa, Campo Grande, Edifício C8, Piso 6, Lisboa 1749-016, Portugal*

We describe solitary wave excitations in a Bose-Fermi mixture loaded in a one-dimensional and strongly elongated lattice. We focus on the mean-field theory under the condition that the fermion number significantly exceeds the boson number, and limit our consideration to lattice amplitudes corresponding to the order of a few recoil energies or less. In such a case, the fermionic atoms display "metallic" behavior and are well-described by the effective mass approximation. After classifying the relevant cases, we concentrate on gap solitons and coupled gap solitons in the two limiting cases of large and small fermion density, respectively. In the former, the fermionic atoms are distributed almost homogeneously and thus can move freely along the lattice. In the latter, the fermionic density becomes negligible in the potential maxima, and this leads to negligible fermionic current in the linear regime.

I. INTRODUCTION

It is widely recognized that optical lattices (OLs) provide a powerful tool to manipulate matter waves, in particular solitons, and to test properties emerging from the interplay between periodicity of the medium and nonlinearity originated by two-body interactions (see, e.g., [1,2] and references therein). OLs are flexible and controllable environments in that they allow one to experimentally create very different regimes, simply by changing the intensity and/or the geometry of laser beams forming the lattice [2]. One such regime in the study of matter waves, already well-understood, is characterized by the smallness of the lattice constant compared to the mean healing length of the Bose-Einstein condensate (BEC) [3,4]. Physical properties in such a regime are determined by the relations among the frequency of the matter-wave, width of the lowest allowed zones, and the width of a gap, in other words by the spectrum of the noninteracting atoms embedded in the lattice. Another matter-wave system studied recently in this way consists of degenerate gases of fermionic atoms trapped in a harmonic potential in the presence of the optical lattice [5]. It has been shown that depending on the Fermi energy, fermionic atoms in an OL can exhibit *either* conducting *or* insulating behavior, and that in the conducting (or metallic) phase, fermionic atoms oscillate symmetrically in the harmonic potential, whereas in the insulating phase, the atoms are trapped on one side of the potential.

The above two cases concern bosons and fermions separately. During the last decade, great progress has been achieved in the experimental realization of Bose-Fermi (BF)

mixtures [6,7]. The coexistence of the two components of such a mixture with different physical properties, as well as the interaction between them, naturally enriches the dynamical properties of each of the components, affecting their stability [8] and leading to a possibility of the existence of solitary waves [9,10]. Dynamical studies have been carried out both for a small number of fermions embedded in a large bosonic component [9,11] and a small number of bosons embedded in a dominant fermionic component [10,12]. In both cases the main theoretical difficulty lies in accounting for the dynamical properties of the fermionic atoms in the mean-field approximation. For the case of a relatively large amount of fermions, the case of interest in this paper, the difficulty has been overcome in Ref. [12] through a description of the fermionic component via a hydrodynamic approximation (used also for the description of a single-component degenerated Fermi gas [13]).

An important property of BF mixtures wherein the fermion component is dominant is that the mixture tends to exhibit essentially three-dimensional character even in a strongly elongated trap. The Pauli exclusion principle results in the extension of the fermion cloud in the transverse direction over distances comparable to the longitudinal dimension of the excitations. It has been shown recently, however, that the quasi-one-dimensional situation can nevertheless be realized in a BF mixture due to strong localization of the bosonic component [10].

Taking into account the effectiveness of the OL in managing systems of cold atoms, their effect on the dynamics of BF mixtures is of obvious interest. Some of the aspects of this problem have already been explored within the framework of the mean-field approximation. In particular, in Ref. [14] the dynamics of the BF mixtures were explored from the point of view of designing quantum dots and in Ref. [15] the existence of vortices in the BF mixtures in the presence of an OL were discussed.

The goal of the present paper is to provide a mean-field description of the dynamics of matter waves in a BF mixture

*Electronic address: bludov@cii.fc.ul.pt

†Electronic address: jayanthi@pas.rochester.edu

‡Electronic address: kenkre@unm.edu

§Electronic address: konotop@cii.fc.ul.pt

of a relatively small number of bosons and a large number of spin-polarized, and thus noninteracting, fermions in a trap elongated in the longitudinal direction, in the presence of a one-dimensional (1D) OL along the longitudinal direction. We will concentrate on a situation where excitations of the mixture have an effective 1D structure, with the characteristic scales in the longitudinal direction significantly exceeding the lattice constant—a situation in which the effective mass approximation is valid for bosons. At the same time, we will explore different regimes for the fermionic component, focusing on cases wherein the Fermi energy exceeds the energy of the lattice barriers, and when the fermionic atoms are well-localized in the lattice minima. We will also explore different conditions for the bosonic component, and in particular consider the cases of relatively deep and shallow lattices, as well as lattices with narrow gaps.

The organization of the paper is as follows. In Sec. II, we describe the statement of the problem and classify possible dynamical regimes of the mixture. In Sec. III, we consider the fermionic system to be in the conducting phase, while the bosons are subjected to a lattice potential with a large band gap. In Sec. IV, we study the case of the bosons being subjected to a lattice potential with a narrow band gap while in Sec. V we consider the situation wherein the lattice potential for the bosons is shallow. In Sec. VI, we investigate the system in which the fermions have moderate density.

II. STATEMENT OF THE PROBLEM

A. Main equations and energetic characteristics

A mixture of bosons with spin-polarized fermions is described by the coupled Heisenberg equations for the field operators (see, e.g., [12])

$$i\hbar\frac{\partial\hat{\Psi}}{\partial t} = -\frac{\hbar^2}{2m_b}\Delta\hat{\Psi} + V_b\hat{\Psi} + g_1\hat{\Psi}^\dagger\hat{\Psi}\hat{\Psi} + g_2\hat{\Phi}^\dagger\hat{\Phi}\hat{\Psi}, \quad (1)$$

$$i\hbar\frac{\partial\hat{\Phi}}{\partial t} = -\frac{\hbar^2}{2m_f}\Delta\hat{\Phi} + V_f\hat{\Phi} + g_2\hat{\Psi}^\dagger\hat{\Psi}\hat{\Phi}. \quad (2)$$

Here $\hat{\Psi}$ and $\hat{\Phi}$ are boson and fermion field operators, respectively, m_b and m_f are masses of bosons and fermions. Two-body interactions of bosons with bosons and fermions are characterized, respectively, by the coefficients $g_1 = 4\pi\hbar^2 a_{bb}/m_b$, and $g_2 = 2\pi\hbar^2 a_{bf}/m$ with $m = m_b m_f/(m_b + m_f)$, a_{bb} and a_{bf} being s-wave scattering lengths for the boson-boson and the boson-fermion interactions, respectively. We will deal with the case where the trap potentials are of the form

$$V_b = \frac{m_b}{2}\omega_b^2(r_\perp^2 + \lambda_b^2 x^2) + U_b(x), \quad (3)$$

$$V_f = \frac{m_f}{2}\omega_f^2(r_\perp^2 + \lambda_f^2 x^2) + U_f(x), \quad (4)$$

where ω_b and ω_f are the linear oscillator frequencies of bosons and fermions in the transverse direction, $r_\perp = (y, z)$,

$\lambda_{b,f}$ are the aspect ratios of the parabolic traps, and $U_{b,f}(x)$ are periodic potentials. The lattice constant d for both the trap potentials will be considered to be the same: $U_{b,f}(x) = U_{b,f}(x+d)$. In particular, we will focus on the case

$$U_b(x) = U_b\cos(2\kappa x) \quad \text{and} \quad U_f(x) = U_f\cos(2\kappa x), \quad (5)$$

where $\kappa = \pi/d$. Also, we assume that the traps are strongly elongated, i.e., $\lambda_{b,f} \ll 1$, and deal with the situation where the fermion number per period N_f (and thus the mean density) is much larger than the number of bosons per period. We emphasize that the last condition does not exclude the possibility for the fermionic density to acquire locally small, and even zero, values. This will naturally affect the choice of analytical approach. However, subject to the weakness of the boson-fermion interactions, in the leading order, the fermion distribution will be described by a static Fermi density, which depends on the spatial variables and is designated below as $n_0(\mathbf{r})$. Being a characteristic of noninteracting fermions, this distribution is characterized by a Fermi energy E_F. Other relevant energy parameters are as follows: the energy of the two-body interactions between the bosons, $g_1 n_b$, and the interactions between a boson and a fermion, $g_2\sqrt{n_b n_f}$ (where $n_{b,f}$ are the respective mean densities of the bosons and the fermions), the transverse energies of the linear oscillators for the bosons, $\hbar\omega_b$, and for the fermions $\hbar\omega_f$, the recoil energy, $E_r = \frac{\hbar^2\kappa^2}{2m_b}$, as well as the energy characterizing the potential depths, $U_{b,f}$.

To reduce the number of parameters, we follow standard practice and measure the energy in the units of the recoil energy E_r introducing $\mathcal{E}_F = E_F/E_r$, $\mathcal{E}_1 = g_1 n_b/E_r$, $\mathcal{E}_2 = g_1 g_2\sqrt{n_b n_f}/E_r$, and $\mathcal{U}_{b,f} = U_{b,f}/E_r$. Then one can distinguish a number of different cases defined by the relations among the energy parameters. In the present paper we deal only with a few of them as summarized in Table I and described in more detail below.

B. Approximations for bosons

The difference in the statistics obeyed by bosons and fermions means that it is appropriate to use different criteria for classification of their respective limiting cases. Given that in the present paper we will deal only with small amplitude excitations of weakly interacting condensates, the boson component is well-described in terms of the effective mass approximation [1,3,4]. We thus exclude the case of large potential barriers and limit our study to moderate barriers, $\mathcal{U}_b \gtrsim 1$ and shallow lattices, $\mathcal{U}_b \ll 1$. We also concentrate on solitary wave solutions. On the one hand their characteristics are determined by the two-body interaction energies, $\mathcal{E}_1$ and $\mathcal{E}_2$, and on the other hand, the spatial localization requires their frequencies [below denoted as ω_0, see Eqs. (19), (37), and (53)] to belong to a gap ΔE of the spectrum of noninteracting bosons (see, e.g., [1]). Therefore the dimensionless gap width, which will be denoted as $\Delta\mathcal{E} = \Delta E/E_r$, is another important characteristic of the bosonic component. When one deals with a shallow lattice, one always has narrow gaps: $\Delta\mathcal{E} \ll 1$. In the case of moderate lattice depth, both cases, narrow gap $\Delta\mathcal{E} \ll 1$ and large gap $\Delta\mathcal{E} \sim 1$, are possible. While the lowest large gap is typical for cosinelike potentials used

TABLE I. Different cases of optical potentials for bosons and fermions addressed in the present paper. For each of the cases for bosonic atoms one can associate one of the cases corresponding to the Fermionic atoms. Here we use the dimensionless variables $\Delta\mathcal{E}$, $\mathcal{E}_F$, $\mathcal{U}_b$, and $\mathcal{U}_f$ for the gap in the linear spectrum of bosons, for Fermi energy, and for amplitudes of the lattice for bosons and for fermions, respectively. For more detailed discussions see the text.

Bosons	Fermions
Moderate lattice: $\mathcal{U}_b \gtrsim 1$, wide gap: $\Delta\mathcal{E} \sim 1$	Large density, $\mathcal{E}_F \gg \mathcal{U}_f$ (Fig. 1 first column)
Moderate lattice: $\mathcal{U}_b \gtrsim 1$, narrow gap: $\Delta\mathcal{E} \ll 1$	Large density, $\mathcal{E}_F \gtrsim \mathcal{U}_f$ (Fig. 1 second column)
Shallow lattice: $\mathcal{U}_b \ll 1$, narrow gap: $\Delta\mathcal{E} \ll 1$	Moderate density, $\mathcal{E}_F \lesssim \mathcal{U}_f$ (Fig. 1 third column)

in most experimental settings, the case of a narrow gap (at the moderate depth) can be achieved either by considering high energies, corresponding to higher bands, or by using a superposition of several laser beams (see the example in Sec. IV).

C. Approximations for fermions

In the present paper we consider the fermionic density to be large enough to justify describing it in the leading order via the Thomas-Fermi (TF) approximation (see, e.g., [8,17])

$$n_0(\mathbf{r}) = \frac{1}{6\pi^2}\left[\frac{2m_f}{\hbar^2}[E_F - V_f(\mathbf{r})]\right]^{3/2} \tag{6}$$

for all $\mathbf{r}$ such that $V_f(\mathbf{r}) \leq E_F$ and $n_0(\mathbf{r}) = 0$ otherwise. In this case, fermionic excitations induced by the interactions be-

tween the two species can be regarded as small perturbations of the spatially inhomogeneous but time-independent background distribution.

Considering the unperturbed distribution of the fermions along the (longitudinal) axis, which is chosen to be x, (i.e., at $r_\perp = 0$), formula (6) gives an idea about three possible cases for the distribution of the fermions (they are illustrated in Fig. 1). Namely, we will say that the density of fermions is large if everywhere along the condensate axis the fermionic density significantly differs from zero (the first and second columns in Fig. 1). Then we still have two possibilities. The first one corresponds to the Fermi energy being much higher than the lattice amplitude, $\mathcal{E}_F \gg \mathcal{U}_f$ [see the first column, Fig. 1(a)] and the difference between the maximal and minimal values of the fermion density is small enough [Fig. 1(b), the first column]. In that case in the leading order we can consider that the fermion density is independent of the longitu-
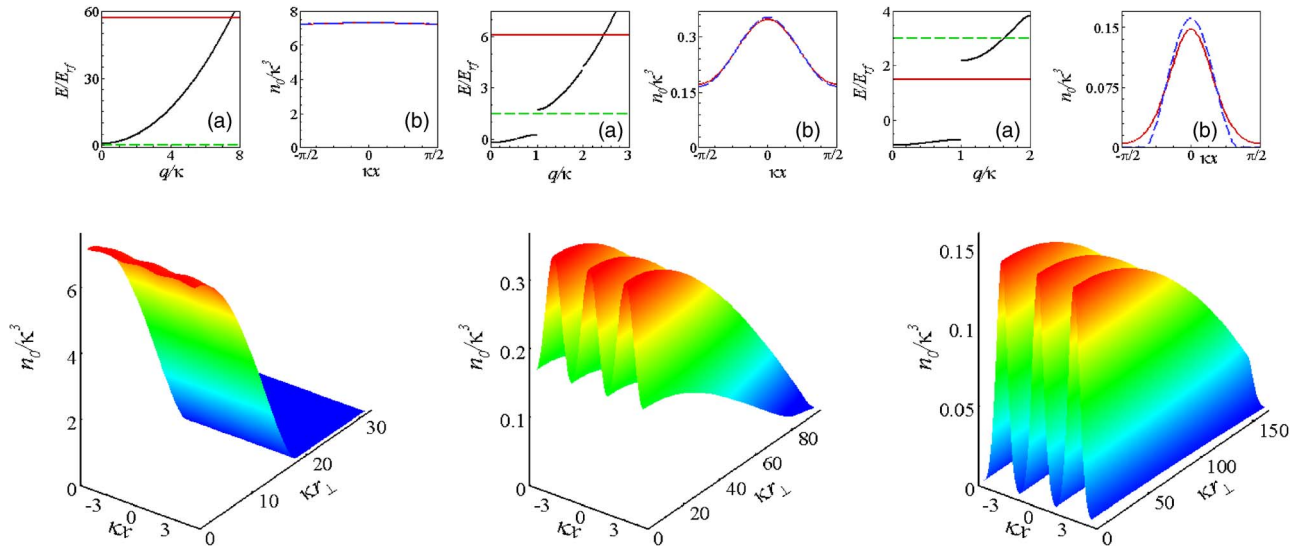

FIG. 1. (Color online) Examples of the distributions of the fermionic atoms considered in the present paper and summarized in Table I. The columns from left to right correspond to $U_f = -0.2E_{rf}$, $a = 0.5d$ (the first column); $U_f = -1.5E_{rf}$, $a = 2.0d$ (the second column); and $U_f = -3.0E_{rf}$, $a = 3.5d$ (the third column). For the sake of convenience the energies are expressed in the units of the fermion recoil energy $E_{rf} = \frac{\hbar^2\kappa^2}{2m_f} = ME_r(M = m_b/m_f)$. Panels (a) show the band structures (extended zones), positions of the Fermi energies (solid red horizontal lines), and energies of the potential barriers for the fermions (dashed green horizontal lines). Panels (b) show the cross sections of spatial distributions of the fermion density at $r_\perp = 0$, computed numerically (solid red curves) and given by the Thomas-Fermi approximation (dashed blue curves) over one period [notice that in panels (b) of the first two columns the difference between the numerical results and the Thomas-Fermi approximation are indistinguishable]. The three-dimensional plots show the spatial distributions of the fermions over three periods. For all three cases considered above, the number of fermions per lattice period is $N_f = 10^4$. Details of the numerical calculations are explained in Appendix A.

dinal coordinate x. The second possibility is shown in the second column of Fig. 1, where the Fermi level is still higher than the OL potential, $\mathcal{E}_F \gtrsim \mathcal{U}_f$ [Fig. 1(a), the second column], but the difference between values of the fermion density at the OL potential maxima and minima is considerable. Then one cannot neglect the x-dependence in the fermion density. In a general situation, both possibilities correspond to the metallic phase of the Fermi component. Indeed, in the first case, the Fermi level falls into one of the upper bands, where gaps are negligibly small. In the second case, the high fermionic density can be achieved by increasing the transverse dimension of the condensate, making the difference between neighboring transverse levels $\hbar\omega_f$ to be less than the upper edge of the largest allowed band (typically of the first lowest band). Then the lowest energy configuration corresponds to partially filled allowed bands in the longitudinal direction and partially filled transverse levels.

Finally, one can have $\mathcal{E}_F \lesssim \mathcal{U}_f$ at some points of the x-axis. This case will be referred to as that of moderate density (see the third column of Fig. 1). In this case, unperturbed fermions constitute an array of independent condensates located in the potential minima.

It is worth pointing out that it can be seen from the insets (b) in Fig. 1 that in the cases of large fermion densities the spatial distributions are very well-described by the TF approximation. Visible differences between the results of the TF approximation and the numerically (exact) computed distributions appear in the case of moderate densities, especially in the vicinities of the OL potential maxima and minima [Fig. 1(b), the third column]. However, the difference between the real TF distribution and the approximate formula (6) is still of order of a few percents of the average distribution. It also does not affect the lattice constant. Therefore in the approximation we will use to treat small-amplitude matter waves (in Sec. VI) the formula (6) will be employed.

D. Dynamical equations

In all the cases considered in the present paper we will neglect the boundary effects of the trap potential in the longitudinal direction. This condition requires the aspect ratios $\lambda_{b,f}$ to be negligibly small, since otherwise the dynamics and even the form of solitary wave excitations can be significantly changed (see, e.g., discussion in [1,10]). We thus impose $\lambda_{b,f}=0$.

Since the energy will be measured in units of the recoil energy, it is natural to introduce the dimensionless variables $\mathbf{R}=\kappa\mathbf{r}$ and $T=\frac{1}{2}a^2\kappa^2\omega_b t$ where $a=\sqrt{\hbar/m_b\omega_b}$ is the transverse linear oscillator length of the bosons, and define the dimensionless macroscopic wave function $\psi(\mathbf{R},T)$ $=(2\sqrt{\pi|a_{bb}|}/\kappa)\Psi(\mathbf{r},t)$, where $\Psi(\mathbf{r},t)=\langle\hat{\Psi}\rangle$, and the dimensionless density of the fermions: $\rho(\mathbf{R},T)$ $=(6\pi^2 M^{3/2}/\kappa^3)n_f(\mathbf{r},t)$, $M=m_b/m_f$, $n_f(\mathbf{r},t)=\langle\hat{\Phi}^\dagger\Phi\rangle$ (the angular brackets stand for the expectation values).

Then the equation governing the evolution of the bosons in terms of the macroscopic wave function is obtained by the standard averaging of Eq. (1), which in dimensionless variables gives (for the details see, e.g., [12])

$$i\frac{\partial\psi}{\partial T}+\Delta_{\mathbf{R}}\psi-\nu_b^2 R_\perp^2\psi-\mathcal{U}_b(X)\psi-2\sigma_1|\psi|^2\psi$$
$$-\sigma_2(1+M)\mathcal{K}_f\rho(\mathbf{R},T)\psi=0. \tag{7}$$

Here after we use the notations $\sigma_{1,2}=\mathrm{sign}(g_{1,2})$, ν_b $=1/(a\kappa)^2$, $\mathcal{K}_f=\frac{2|a_{bf}|\kappa}{3\pi M^{3/2}}$, and $\rho(\mathbf{R},T)=\rho_0(\mathbf{R})+\delta\rho(\mathbf{R},T)$, where $\rho_0(\mathbf{R})$ and $\delta\rho(\mathbf{R},T)$ are the stationary (background) density and local perturbation of density of the fermions, respectively.

A degenerate fermionic gas can be described in terms of the Landau theory of quasiparticles excited in the vicinity of the Fermi surface and is governed by the hydrodynamic approximation. The respective equation for the local density of quasiparticles can be derived directly from Eq. (2) (this is done in Ref. [12]) and in dimensional variables reads

$$\frac{\partial^2\delta\rho}{\partial T^2}=\nabla_{\mathbf{R}}\cdot\left[\rho_0\nabla_{\mathbf{R}}\left(\frac{4M}{3\rho_0^{1/3}}\delta\rho+\chi\sigma_2|\psi|^2\right)\right]. \tag{8}$$

Here we have introduced the dimensionless density in the TF approximation

$$\rho_0=\left[\mathcal{E}_F-\nu_f^2 R_\perp^2-\mathcal{U}_f(X)\right]^{3/2}, \tag{9}$$

and defined the parameters $\nu_f=\omega_f\nu_b/(\omega_b M^{1/2})$ and χ $=2|a_{bf}/a_{bb}|(1+M)M$.

To complete the statement of the problem we now introduce the normalization conditions. We will be interested in bright and dark soliton solutions and therefore we distinguish the normalization conditions for the bosons of the two types. In the case of spatially localized distribution of the bosons (the case of bright solitons) we impose the standard normalization condition

$$\int|\psi|^2 d\mathbf{R}=\mathcal{N}_b, \quad \mathcal{N}_b=4\pi|a_{bb}|\kappa N_b, \tag{10}$$

where N_b is the total number of bosons and the integral is over the whole space. Formally, a dark soliton solution is constructed against an infinite background, and therefore the normalization condition must be written down for the background solution in the absence of the soliton. The condition is

$$\int d\mathbf{R}_\perp\int_{-\pi/2}^{\pi/2}dX|\psi|^2=\mathcal{N}_{b0}, \quad \mathcal{N}_{b0}=4\pi|a_{bb}|\kappa N_{b0}, \tag{11}$$

where $\mathcal{N}_{b0}=4\pi|a_{bb}|\kappa N_{b0}$ and N_{b0} is an average number of bosons per OL period.

We will similarly impose the normalization for the background of the fermionic component as

$$\int d\mathbf{R}_\perp\int_{-\pi/2}^{\pi/2}dX\,\rho_0=6\pi^2 M^{3/2}N_f, \tag{12}$$

where N_f is an average number of fermions in a unit cell.

III. FERMIONS AT LARGE DENSITIES WITH BOSONS IN A LATTICE WITH A LARGE GAP

A. Scaling

Let us start with a moderate size lattice having a wide gap for bosons and with large density of fermions. This is represented by the first line in Table I and illustrated in the left column in Fig. 1. We introduce characteristic scales of the transverse distribution of the bosons and the fermions: For the former, $R_b = 1/\sqrt{\nu_b}$, which, in dimensionless units, corresponds to the transverse oscillator length of the low density boson component; and for the latter, $R_f = \sqrt{\mathcal{E}_F}/\nu_f$, which follows from Eq. (9). Here, we restrict our considerations to the potential barrier being of the order of a few recoil energies, i.e., $\mathcal{U}_f \sim 1$. This means that $\mathcal{E}_F \gg 1$ (see Table I). Considering the linear oscillator frequencies of the bosons and the fermions to be of the same order of magnitude, $\nu_f \sim \nu_b$, we obtain the relation $R_f \gg R_b$. On defining the small parameter $\epsilon = \frac{a}{\xi} \ll 1$, where $\xi = (8\pi n_b |a_{bb}|)^{-1/2}$ (n_b is the maximal density of bosons), and requiring [10] $R_f^2/R_b^2 \sim \mathcal{E}_F/\nu_f = \varepsilon_F/(\nu_f \epsilon^2)$, where $\varepsilon_F \gtrsim 1$ is a parameter of the problem, we can rewrite Eq. (9) with accuracy $O(\epsilon^3)$ as

$$\rho_0 \approx \mathcal{E}_F^{3/2}\left[1 - \frac{3\epsilon^2}{2\varepsilon_F}[\nu_f^2 R_\perp^2 + \mathcal{U}_f \cos(2X)]\right]. \quad (13)$$

At this point we observe that ξ used in the definition of the small parameter is nothing but the healing length when one deals with dark soliton excitations or sound waves. If, however, bright matter solitons are under considerations, when the conventional definition of the healing length is not appropriate, ξ is of order of the mean soliton width. The scaling introduced above allows us to concentrate on the spatial domain, limited in the transverse direction by some radius $\tilde{R}$, which satisfies the condition $R_b \ll \tilde{R} \ll R_f$ (i.e., by the domain in the transverse direction, where the bosonic component decays while the fermionic component changes insignificantly). Specifically, we impose $\tilde{R} = \epsilon^{-1/2}$.

B. Multiple-scale expansion and 1D equations

Following standard multiple-scale analysis (see, e.g., [1,10]), we introduce scaled quantities $t_j = \epsilon^j T$ and $x_j = \epsilon^j X$, regarded as independent variables, and look for a solution in the form of the series

$$\psi(\mathbf{R}, T) = \epsilon \psi_1 + \epsilon^2 \psi_2 + \epsilon^3 \psi_3 + O(\epsilon^4). \quad (14)$$

Moreover, it is clear from Eq. (8) that $\delta\rho \sim |\psi|^2$. Using the expansion for ψ in the form of Eq. (14), we find that the value $\delta\rho$ is of the order ϵ^2. In other words, $\delta\rho = \epsilon^2 \rho_1$, where $\rho_1 \sim |\psi_1|^2$.

Substituting the above expansions into Eq. (7) and gathering the terms of the same order in ϵ, we rewrite Eq. (7) in the form of a set of equations [1,3,10]:

$$\left(i\frac{\partial}{\partial t_0} - \mathcal{L}\right)\psi_j = F_j, \quad (15)$$

where F_j's are given in Appendix B and depend only on ψ_i with $i < j$, and the operator $\mathcal{L}$ is given by

$$\mathcal{L} \equiv \mathcal{L}_\perp + \mathcal{L}_x + \sigma_2(1 + M)\mathcal{K}_f \mathcal{E}_F^{3/2}, \quad (16)$$

where

$$\mathcal{L}_\perp = -\Delta_\perp + \nu_\perp^2 R_\perp^2,$$

$$\nu_\perp^2 = \nu_b^2 - \sigma_2 \frac{3}{2}(1 + M)\mathcal{K}_f \sqrt{\mathcal{E}_F}\nu_f^2, \quad (17)$$

$$\mathcal{L}_x = -\frac{\partial^2}{\partial x_0^2} + \mathcal{U}(x_0),$$

$$\mathcal{U}(x_0) = \mathcal{U}_b(x_0) - \sigma_2 \frac{3}{2}(1 + M)\mathcal{K}_f \sqrt{\mathcal{E}_F}\mathcal{U}_f(x_0). \quad (18)$$

For the next consideration it is important that the scaling chosen guarantees that $\nu_\perp > 0$.

We look for a solution to Eq. (7) which describes a Bloch function weakly modulated by the nonlinearity present in the two-body interactions. Such a solution can be sought in the form

$$\psi_1 = A(x_1, t_1)\phi_n(x_0)\zeta(R_\perp)e^{-i\omega_0 t_0}, \quad (19)$$

restricting our considerations to states bordering on the edge of the first gap (i.e., here either $n=0$ or $n=1$). Note that $\phi_n(x_0)$ and $\zeta(R_\perp)$ are defined in Appendix B. The envelope function $A(x_1, t_1)$ depends on the slow variables, $(x_1, x_2, \ldots, t_1, t_2, \ldots)$, from which only the most rapid are indicated explicitly. The envelope function is independent of x_0, t_0, and $R_\perp$.

Direct substitution leads to the verification that the ansatz (19) satisfies the first ($j=1$) of Eq. (15) provided

$$\omega_0 = \sigma_2(1 + M)\mathcal{K}_f \mathcal{E}_F^{3/2} + \varepsilon_n + 2\nu_\perp. \quad (20)$$

Taking into account the wave nature of the discussed phenomena throughout this paper ω_0 will be referred to as a frequency (notice, however, that in the dimensionless units it also can be interpreted as energy or chemical potential, whenever one speaks about stationary solutions).

Proceeding to the second order of expansion, i.e., to the computation of ψ_2, one verifies that it cannot be made zero for any time. We thus impose a constraint for the density of bosons to be slowly dependent on time (i.e., to be independent on t_0). To this end ψ_2 must be searched in the form

$$\psi_2 = \sum_{n' \neq n} B_{n'}(x_1, t_1)\phi_{n'}(x_0)\zeta(R_\perp)\exp(-i\omega_0 t_0). \quad (21)$$

Substituting this expansion into the second order equation from Eq. (15), and eliminating secular terms by requiring F_2 to be orthogonal to $\phi_n(x)$, we find that the envelope function A is independent of t_1, i.e., $A = A(x_1, t_2)$. Furthermore,

$$\psi_2 = \frac{\partial A}{\partial x_1}\sum_{n' \neq n}\frac{\Gamma_{n'n}}{\varepsilon_n - \varepsilon_{n'}}\phi_{n'}(x_0)\zeta(R_\perp)e^{-i\omega_0 t_0}, \quad (22)$$

where

$$\Gamma_{n'n} = -2\int_{-\pi/2}^{\pi/2}\phi_{n'}(x)\frac{d}{dx}\phi_n(x)dx. \quad (23)$$

On the other hand, because the equation of the third order involves a dependence on the fermion density, it must be solved together with Eq. (8). Since the value $|\psi_1|^2$ depends upon t_2, i.e., changes slowly in time, we can find the particular solution of Eq. (8) in the static limit approximation (where $\partial^2\rho_1/\partial T^2 = 0$) in the form

$$\rho_1 = -\sigma_2\gamma|A(x_1,t_2)|^2|\phi_n|^2\zeta^2, \qquad (24)$$

where $\gamma = 3\chi\sqrt{\mathcal{E}_F}/(4M)$. Here we have used the fact that from Eq. (13), $\frac{1}{\rho_0}\left|\frac{\partial\rho_0}{\partial X}\right| \ll 1$ and therefore in the leading order in Eq. (8) we can neglect the dependence of ρ_0 upon the spatial coordinates.

Comparing the result (24) with the explicit form of ψ_1 from Eq. (19), we find that the same envelope function ρ_1 governs both the local fermion density and the boson density. Substituting Eq. (24) in F_3 (see Appendix B) and requiring the absence of secular terms in the third order equation of the multiple scale expansion (i.e., requiring the orthogonality of F_3 and ψ_1), we find that $A(x_1,t_2)$, satisfies the NLS equation

$$i\frac{\partial A}{\partial t_2} + \frac{1}{2\mathcal{M}}\frac{\partial^2 A}{\partial x_1^2} + \chi_n|A|^2A = 0. \qquad (25)$$

In this NLS equation,

$$\frac{1}{2\mathcal{M}} = 1 + \sum_{n'\neq n}\frac{|\Gamma_{n'n}|^2}{\varepsilon_n - \varepsilon_{n'}} \approx \frac{1}{2}\left(\frac{\partial^2\varepsilon_{n,q}}{\partial q^2}\right)_{q=1}, \qquad (26)$$

$$\chi_n = \frac{\nu_\perp}{\pi}\left(\frac{\mathcal{E}_F^{1/2}(1+M)^2|\kappa a_{bf}|^2}{2\pi M^{3/2}|\kappa a_{bb}|} - \sigma_1\right)\times\int_{-\pi/2}^{\pi/2}|\phi_n(x)|^4dx, \qquad (27)$$

the quantity $\varepsilon_{n,q}$ being defined in Appendix B. The effective mass $\mathcal{M}$ characterizes the response of the bosons to the OL potential—its expression through the dispersion relation can be obtained by the so-called **kp** method [18–21]; see also [3].

C. Bose-Fermi gap solitons

The NLS equation given in Eq. (25) is the main result of our analysis. To check its experimental feasibility, let us consider an example of a Rb^{87}-K^{40} mixture with characteristics given in Ref. [6], in a trap with a radial size $a\sim 2$ μm and OL with a period $\pi/\kappa\sim 1$ μm. Taking the number of rubidium atoms to be 500, and the scattering lengths a_{bb} =2 nm and a_{bf}=11 nm [16] providing $\chi_n>0$, we obtain that the width of the bright soliton is $\xi\approx 14$ μm [see the comment after Eq. (13)]. This gives $\epsilon=0.14$. From Fig. 1 (the first column) after taking into account that the energies are measured in units of the fermion recoil energy E_{rf}, and the ratio between the fermion and the boson recoil energies is given by $E_{rf}/E_r=M\approx 2.17$ for the Rb^{87}-K^{40} condensate, we also compute $\mathcal{E}_F\approx 124.2\gg 1$. Thus $\varepsilon_F\approx 2.43$, which is in agreement with the imposed condition $\varepsilon_F\gtrsim 1$ [see formula (13)].

It follows from Eq. (18) that, in a BF mixture, the presence of the fermions can change the effective periodic poten-
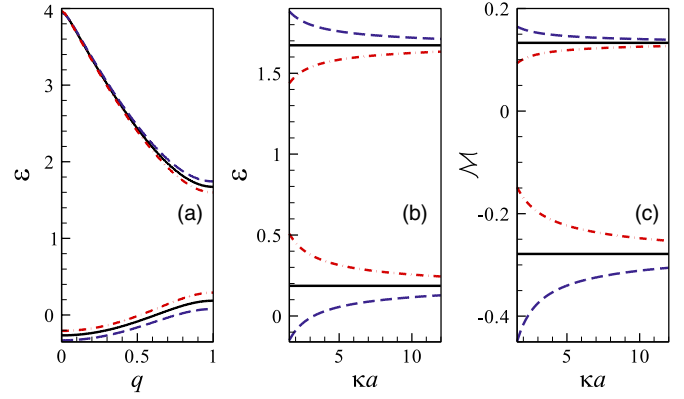

FIG. 2. (Color online) (a) The bosonic band structure (reduced zones) for the two lowest energy bands in the case where the transverse linear oscillator length $a=2.0d$. (b) The dependence of the edges of the bosonic band gap ($q=1$) on the transverse linear oscillator length a. (c) The dependence of the effective mass $\mathcal{M}$ at the edges of the bosonic band gap ($q=1$) on the transverse linear oscillator length a. These dependencies were computed for the Rb^{87}-K^{40}, mixture where $|a_{bf}|=0.02d$, $N_f=10^4$ per period, $\mathcal{U}_f=-3.0$, $\mathcal{U}_b=-1.5$, and for the cases when the boson-fermion interactions are absent (solid black curves), are repulsive (dashed-and-dot red curves), and are attractive (dashed blue curves).

tial for the bosons, and, consequently, the value of the gap width $\Delta\mathcal{E}$. This effect is illustrated in Fig. 2(a). Thus if the interaction between bosons and fermions is repulsive (σ_2 =1), the boson-fermion interaction leads to a decrease in the potential barrier for the bosons. As a result, the value of the gap width becomes narrower in comparison with the situation in which $\chi=0$. In the opposite case, when the boson-fermion interaction is attractive ($\sigma_2=-1$), there is an increase in the effective potential barrier for the bosons. In turn, the gap becomes wider in comparison with the $\chi=0$ case.

The BF mixture also exhibits another interesting property which we illustrate in Fig. 2(b): one can change the effective potential barrier for bosons by changing the transverse oscillator length. When the transverse linear oscillator length a is increased (the linear oscillator frequency ω_b is decreased), the value of $E_\perp$ decreases. Since ω_f is of the same order as ω_b ($\nu_f\sim\nu_b$), this can lead to the lowering of the Fermi energy $\mathcal{E}_F$. Equation (18) shows that this, in turn, can result in increasing or decreasing the effective potential barrier and gap width for bosons when σ_2 equals 1 or −1, respectively. It should be mentioned that in the limit $a\to\infty$, the value of the effective potential for bosons tends to $\mathcal{U}_b$, i.e., to the value in the absence of the boson-fermion interaction. The absolute value of the effective mass $\mathcal{M}$ [see Fig. 2(c)] decreases (in the case of the attractive boson-fermion interaction $\sigma_2=-1$) or increases (in the case of the repulsive boson-fermion interaction $\sigma_2=1$) with an increase in the transverse linear oscillator length a. This is a remarkable finding of our analysis. This means that one can change the band gap properties of the bosons by changing the transverse oscillator frequency.

When the boson-fermion interaction is turned off ($\chi=0$), the boson and the fermion components are independent of each other: the fermion density is given by the TF approximation, Eq. (9), and the boson system is described by the

NLS equation. When $\chi \neq 0$, the boson-fermion interactions always lead to attractive interactions between the bosons. This consequence of our present analysis is in qualitative agreement with earlier results [8,10,12]. One can easily find the critical value of the boson-fermion interaction at which both interactions are balanced, i.e., when $\chi_n = 0$:

$$|a_{bf}^{cr}| = \left[\frac{\pi}{\kappa} \frac{2|a_{bb}|}{\mathcal{E}_F^{1/2}} \frac{M^{3/2}}{(1+M)^2} \right]^{1/2}. \qquad (28)$$

When $|a_{bf}|$ equals the critical value, the system becomes an ideal gas, described by the linear Schrödinger equation. If $|a_{bf}|$ is larger than the above critical value, $\chi_n > 0$, the interaction between bosons and fermions dominates, leading to an effective attractive interaction between the bosons.

As mentioned above, in the case of periodic lattices, the value of the effective mass can be either positive or negative depending on the region of the Brillouin (reduced) zone [see Fig. 2(c)]. Therefore formation of a bright soliton is possible if $\mathcal{M} \cdot \chi_n > 0$. For the example of the Rb^{87}-K^{40} mixture shown in Fig. 2, small amplitude bright solitons can be created in the vicinity of the edges $\varepsilon_0 = 0.18$ ($\mathcal{M} = -0.28$) and $\varepsilon_1 = 1.67$ ($\mathcal{M} = 0.13$), for $\chi_n < 0$ and $\chi_n > 0$, respectively. An explicit form of the respective solution is obtained directly from Eq. (25) and in dimensionless variables can be written down as follows:

$$|\psi|^2 = \mathcal{A}_b \, \mathrm{sech}^2\left(\frac{X}{\ell_{bs}} \right) |\phi_n(X)|^2 e^{-\nu_\perp R_\perp^2}, \qquad (29)$$

$$\rho = \rho_0 - \sigma_2 A_f \, \mathrm{sech}^2\left(\frac{X}{\ell_{bs}} \right) |\phi_n(X)|^2 e^{-\nu_\perp R_\perp^2}. \qquad (30)$$

Here

$$A_b = \frac{\nu_\perp}{\pi \ell_{bs}^2 \chi_n \mathcal{M}} \quad \text{and} \quad A_f = \gamma A_b \qquad (31)$$

are the amplitudes of the modulations of density profiles for the bosons and the fermions and ℓ_{bs} characterizes the width of the soliton and parametrizes the family of the solutions. A convenient parametrization useful in experimental applications is given by the total number of bosons, which can be done using the normalization condition (10). To this end, taking into account that $\phi_n(X)$ is normalized and is a rapidly varying function with respect to the soliton envelope), we obtain, in leading order, the link

$$\ell_{bs} = \frac{2}{\pi \mathcal{N}_b \chi_n \mathcal{M}}. \qquad (32)$$

In the vicinity of the edges $\varepsilon_0 = 0.18$ ($\mathcal{M} = -0.28$) and $\varepsilon_1 = 1.67$ ($\mathcal{M} = 0.13$) (see the example shown in Fig. 2) a dark soliton can be excited if $\chi_n > 0$ and $\chi_n < 0$, respectively. The explicit form of the two-component dark soliton solution reads

$$|\psi|^2 = A_b \tanh^2\left(\frac{X}{\ell_{ds}} \right) |\phi_n(X)|^2 e^{-\nu_\perp R_\perp^2}, \qquad (33)$$

$$\rho = \rho_0 - \sigma_2 A_f \tanh^2\left(\frac{X}{\ell_{ds}} \right) |\phi_n(X)|^2 e^{-\nu_\perp R_\perp^2}, \qquad (34)$$

where

$$A_b = \frac{\nu_\perp}{\pi} \frac{1}{\ell_{ds}^2 |\chi_n \mathcal{M}|} \quad \text{and} \quad A_f = \gamma A_b. \qquad (35)$$

The link between the soliton width ℓ_{ds} and the number of particles per unit cell follows from Eq. (11)

$$\ell_{ds} = \frac{1}{\sqrt{\mathcal{N}_{b0} |\chi_n \mathcal{M}|}}. \qquad (36)$$

Formally, the expressions for the bright and the dark solitons coincide with known formulas for the gap solitons in a single-component bosonic condensate (see, e.g., [1–3]). These solutions have essentially different properties since they constitute only a part of the two-component soliton, the second component being a fermionic excitation. As we can see, the bright and the dark soliton solutions are possible for both the boson and the fermion components depending upon the sign of interactions and the effective mass. When the interaction between bosons and fermions is attractive ($\sigma_2 = -1$), we show that both the components can show simultaneous increase (decrease) in their densities. By contrast, in the case of repulsive interactions ($\sigma_2 = 1$) between the components, there is an increase of the density of one component while that of the other decreases.

The above-mentioned difference from the single-component bosonic condensate stems from the fact that the fermionic distribution *creates an effective medium* for the bosonic solitons. This distribution is very sensitive to the transverse confinement of the condensate [as illustrated in Figs. 2(b) and 2(c)], and thus can be effectively governed by variation of the transverse linear oscillator frequency. In particular, by increasing the confinement in the transverse direction, one can increase the Fermi energy $\mathcal{E}_F$, thus allowing for the effective nonlinearity for bosons χ_n to change the sign [see Eq. (27)] and consequently to change the type of the soliton.

IV. FERMIONS AT LARGE DENSITIES WITH BOSONS IN A LATTICE WITH AN ARROW GAP

A. Dynamical equations

Now we consider the excitations of a BF mixture in a deep lattice for bosons with a narrow band gap. This situation can be realized either when the frequency of the bosonic wave function is large enough or when the OL is created by laser beams of more than one frequency. To illustrate the first possibility, we present an example of the potential in Fig. 3. Alternatively, the fermionic component can originate potentials with an arrow gap (see the discussion in Sec. VI). The expansion provided in the previous section cannot be used for this case since one has to take into account coupling between Bloch states corresponding to the different edges of the gap. This coupling is due to the nonlinear interactions and arises similarly to the situation of gap solitons in photo-
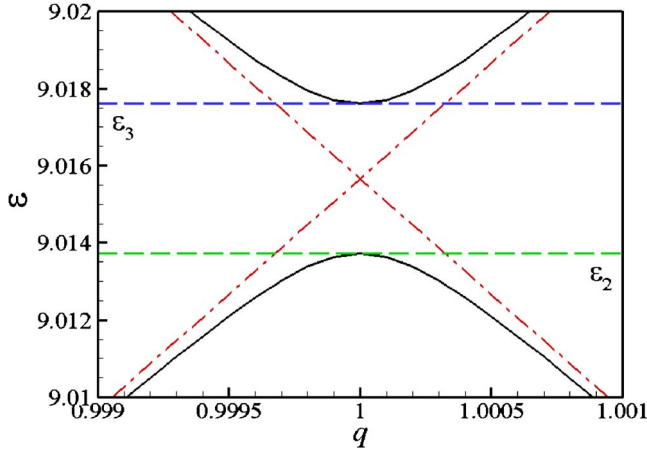
FIG. 3. (Color online) An example of the band structure with a narrow band gap between bands $n=2$ and $n=3$ (solid black lines). Here $\Delta\mathcal{E}\approx 0.004$ and the potential is $\mathcal{U}_b=-\cos(2X)$. The dispersion curves for the case without OL are depicted by red dash-and-dot curves. The horizontal dashed curves (green and blue) represent the upper boundary of the $n=2$ band and the lower boundary of the $n=3$ band, respectively.

nic crystals [22] or in nonlinear discrete systems [23]. To be specific, we assume that a narrow gap is created between the two bands $n=2$ and $n=3$: $\Delta\mathcal{E}=|\varepsilon_3-\varepsilon_2|\ll|\varepsilon_{2,3}|$ where ε_2 and ε_3 are the upper boundary of the $n=2$ band and the lower boundary of the $n=3$ band (see Fig. 3). Using the expansion as shown in [22,23], we look for a solution to Eq. (7) in the form [cf. Eq. (15)]

$$\psi_1 = [A_2(x_1,t_1)\phi_2 + A_3(x_1,t_1)\phi_3]\zeta e^{-i\omega_0 t_0}. \tag{37}$$

Here, as before, $A_n(x_1,t_1)$ $(n=2,3)$ are functions of slow variables, ζ and ϕ_n are given in Appendix B, and ω_0 is referred to as a frequency of the soliton. Expression (37) describes the superposition of the modes bordering the narrow bosonic gap. Using the ansatz (37), in the first order of ϵ $(j=1)$ for the bosons, we find from Eq. (15) at $j=1$

$$\omega_0 = \sigma_2(1+M)\mathcal{K}_f \mathcal{E}_F^{3/2} + \widetilde{\varepsilon} + 2\nu_\perp, \tag{38}$$

where $\widetilde{\varepsilon}=(\varepsilon_0+\varepsilon_1)/2$ [cf. Eq. (20)].

For the next order, we expand ψ_2 over the complete set of the eigenfunctions of the operator $\mathcal{L}$ [cf. Eq. (21)]

$$\psi_2 = \left[B_2\phi_2 + B_3\phi_3 + \sum_{n\neq 2,3} B_n\phi_n \right]\zeta e^{-i\omega_0 t_0}, \tag{39}$$

where $B_n=B_n(x_1,t_1)$. Substituting Eq. (37) and the last representation in Eq. (15) with $j=2$, we obtain

$$\sum_{n'} (\widetilde{\varepsilon}-\varepsilon_{n'})B_{n'}\phi_{n'} = -i\frac{\partial A_2}{\partial t_1}\phi_2 - 2\frac{\partial A_2}{\partial x_1}\frac{\partial\phi_2}{\partial x_0} - i\frac{\partial A_3}{\partial t_1}\phi_3$$
$$- 2\frac{\partial A_3}{\partial x_1}\frac{\partial\phi_3}{\partial x_0}.$$

The fact that the right-hand side of this equation must be orthogonal to ϕ_2 and ϕ_3 yields the two equations

$$\frac{\partial A_2}{\partial t_1} - iv\frac{\partial A_3}{\partial x_1} = 0, \qquad \frac{\partial A_3}{\partial t_1} + iv\frac{\partial A_2}{\partial x_1} = 0, \tag{40}$$

where $v=\Gamma_{32}$ is the group velocity of the mode $\phi_2+i\phi_3$ in the limit of the closed gap. For a discussion of this point, see, e.g., [22,23]. The further requirement of the orthogonality between ψ_1 and ψ_2 yields the relation $\overline{A}_2 B_2 + \overline{A}_3 B_3 = 0$ (here and henceforth in this paper an overbar stands for complex conjugation). It follows from the system (40) that slowly varying amplitudes are related to each other as $A_2 = \pm iA_3$, which readily gives the link between B_2 and B_3: $B_2 = \mp iB_3$. Consequently, from Eq. (40), it follows that $A_{2,3}$ depending on $x_1 \mp vt_1$.

Let us now fix the direction of propagation of the solution by choosing the dependence on $\widetilde{x}=x_1-vt_1$. This corresponds to the branch with $A_2=-iA_3$ and $B_2=iB_3$, which means that the second order term acquires the form:

$$\psi_2 = \left[(\phi_2-i\phi_3)B_2 + \sum_{n\neq 2,3} \frac{\Gamma_{n2}-i\Gamma_{n3}}{\widetilde{\varepsilon}-\varepsilon_n}\phi_n\frac{\partial A_2}{\partial\widetilde{x}} \right]\zeta e^{-i\omega_0 t_0}.$$

Similar to the previous case, we solve Eq. (8) for the fermion density ρ_1. After substituting ψ_1 from Eq. (37), we obtain

$$\rho_1 = -\sigma_2\gamma|\phi_2+i\phi_3|^2|\zeta|^2|A_2|^2. \tag{41}$$

From Eqs. (37) and (41), we see that both ψ_1 and ρ_1 are now determined by the single envelope function A_2.

Using the above result for ρ_1 in the third order equation of the multiple scale expansion, i.e., in Eq. (15) with $j=3$, and requiring orthogonality of F_3 and ψ_1 we find that A_2 satisfy the following system of equations:

$$i\frac{\partial A_2}{\partial t_2} - iv\frac{\partial A_2}{\partial x_2} + (D_{22}-iD_{23})\frac{\partial^2 A_2}{\partial\widetilde{x}^2} + \chi_2|A_2|^2 A_2$$
$$= -i\frac{\partial B_2}{\partial t_1} - iv\frac{\partial B_2}{\partial\widetilde{x}}, \tag{42}$$

$$i\frac{\partial A_2}{\partial t_2} - iv\frac{\partial A_2}{\partial x_2} + (D_{33}+iD_{32})\frac{\partial^2 A_2}{\partial\widetilde{x}^2} + \chi_3|A_2|^2 A_2$$
$$= i\frac{\partial B_2}{\partial t_1} + iv\frac{\partial B_2}{\partial\widetilde{x}}, \tag{43}$$

where

$$D_{lm} = \delta_{lm} + \sum_{n\neq 2,3}\frac{\Gamma_{ln}\Gamma_{mn}}{\widetilde{\varepsilon}-\varepsilon_n},$$

and

$$\chi_l = \frac{\nu_\perp}{\pi}\left(\frac{\mathcal{E}_F^{1/2}(1+M)^2|\kappa a_{bf}|^2}{2\pi M^{3/2}|\kappa a_{bb}|} - \sigma_1\right)\int_{-\pi/2}^{\pi/2}(\phi_2^2+\phi_3^2)\phi_l^2 dx_0.$$

Here we have taken into account for symmetric potentials $\phi_0(X)$ and $\phi_1(X)$ are real and have different parities.

Taking into account that in a typical case $\chi_2\approx\chi_3$, and using the relation between A_2 and A_3, the variables B_2 and B_3 can be determined from Eqs. (42) and (43)

$$B_3 = -iB_2 = -\frac{D_{22} - D_{33} - 2iD_{23}}{4v}\frac{\partial A_2}{\partial \tilde{x}}. \qquad (44)$$

Using this in Eqs. (42) and (43), the evolution equation for the envelope A_2 takes the form of the NLS equation

$$i\frac{\partial A_2}{\partial t_2} + \frac{1}{2\mathcal{M}}\frac{\partial^2 A_2}{\partial \tilde{x}^2} + \chi_2|A_2|^2 A_2 = 0, \qquad (45)$$

where the effective mass $\mathcal{M}$ is determined by

$$\frac{1}{\mathcal{M}} = D_{22} + D_{33} = \frac{1}{2}\left(\frac{\partial^2 \varepsilon_{2,q}}{\partial q^2}\right)_{q=1} + \frac{1}{2}\left(\frac{\partial^2 \varepsilon_{3,q}}{\partial q^2}\right)_{q=1}. \qquad (46)$$

Equation (46) shows that the effective mass is determined by the influence of the remaining Bloch states of the periodic lattice potential on the two given states (in the case under consideration ε_2, ε_3) and also by the mutual influence of these two states.

B. Coupled gap solitons and discussion of the results

As in the previous case existence of bright and dark solitons is determined by the sign of $\chi_2\mathcal{M}$. If $\chi_2\mathcal{M} > 0$, one can obtain a bright soliton solution in the form

$$\left||\psi|\right|^2 = \frac{1}{4}A_b \operatorname{sech}^2\left(\frac{X - vT}{2\ell_{bs}}\right)[|\phi_2(X)|^2 + |\phi_3(X)|^2]e^{-\nu_\perp R_\perp^2}, \qquad (47)$$

$$\rho = \rho_0 - \frac{\sigma_2}{4}A_f \operatorname{sech}^2\left(\frac{X - vT}{2\ell_{bs}}\right)[|\phi_2(X)|^2 + |\phi_3(X)|^2]e^{-\nu_\perp R_\perp^2}, \qquad (48)$$

where $A_{b,f}$ and ℓ_{bs} are given by Eqs. (31) and (32) (with χ_n substituted by χ_2). If $\chi_2\mathcal{M} < 0$ one obtains a dark soliton solution

$$|\psi|^2 = \frac{1}{2}A_b \tanh^2\left(\frac{X - vT}{\sqrt{2}\ell_{ds}}\right)[|\phi_2(X)|^2 + |\phi_3(X)|^2]e^{-\nu_\perp R_\perp^2}, \qquad (49)$$

$$\rho = \rho_0 - \frac{\sigma_2}{2}A_f \tanh^2\left(\frac{X - vT}{\sqrt{2}\ell_{ds}}\right)[|\phi_2(X)|^2 + |\phi_3(X)|^2]e^{-\nu_\perp R_\perp^2}, \qquad (50)$$

where $A_{b,f}$ and ℓ_{ds} are given by Eqs. (35) and (36), respectively.

We thus see that the result obtained here is qualitatively different from that obtained in the previous section, i.e., from single-mode gap solitons. First of all, a small gap results in coupling of the modes, which makes it impossible to obtain a static solution [24]. Instead, soliton solutions are constructed against a background moving with the velocity v corresponding to the group velocity of the carrier wave $\phi_2 + i\phi_3$. For instance, for a potential whose band gap is illustrated in Fig. 3, the group velocity v is equal to $v \approx 5.988$. Second, the absolute value of the effective mass is bigger than in the case of single-mode gap solitons, since it is given by the differ-

ence of the effective masses associated with the two gap edges [see Eq. (46)] (the effective mass $\mathcal{M}$ for the potential of Fig. 3 is equal to $\mathcal{M} \approx 0.49$). Finally, we notice that the spatial structure of the carrier wave is weakly pronounced in the case at hand, since in a typical situation $(|\phi_2(X)|^2 + |\phi_3(X)|^2)$ is weakly dependent on the spatial coordinate.

V. FERMIONS AT LARGE DENSITIES WITH BOSONS IN A SHALLOW LATTICE

Let us now pass to the case of a shallow OL, where $\mathcal{U}_b \ll 1$, an example of which is shown in Fig. 1 (the left column). Now the periodic modulation itself must be considered as a perturbation (so, $\mathcal{U}_{b,f} = \epsilon^2 u_{b,f}$) and one has to modify the multiple-scale expansion. This situation is also well-known in the theory of photonic crystals [25].

In this case, in the multiscale expansion scheme we will seek the solution for $\psi(\mathbf{R}, T)$ in the form of the series

$$\psi(\mathbf{R}, T) = \epsilon\psi_1 + \epsilon^3\psi_3 + O(\epsilon^4). \qquad (51)$$

At the same time the series for $\rho(\mathbf{R}, T) = \rho(\mathbf{R}) + \epsilon^2\rho_1(\mathbf{R}, T)$ remains valid. Notice that for a shallow lattice in Eq. (51) the term proportional to the second power of ϵ is absent [cf. Eq. (14)]. The set of equations, obtained from the multiscale expansion (15) will be modified. First, the operator $\mathcal{L}_x$ is given by $\mathcal{L}_x = -\frac{\partial^2}{\partial x_0^2}$ [cf. Eq. (18)]. Second, the equation with $j=3$ appears as the second order approximation (there is no equation with $j=2$). Finally, now F_3 is given by

$$F_3 = -i\frac{\partial\psi_1}{\partial t_2} - \frac{\partial^2\psi_1}{\partial x_1^2} - 2\frac{\partial^2\psi_1}{\partial x_0\,\partial x_2} + u\cos(2x_0)\psi_1 + 2\sigma_1|\psi_1|^2\psi_1 + \sigma_2(1 + M)\mathcal{K}_f\rho_1\psi_1, \qquad (52)$$

with $u = u_b - 3\sigma_2(1 + M)\mathcal{K}_f\sqrt{\mathcal{E}_F}u_f/2$. As we can see from Eq. (52), the information about the OL potential u appears in a multiscale equation of the third order. As a consequence, the macroscopic wave function for the bosons is given by a weakly modulated superposition of two counterpropagating plane waves:

$$\psi_1 = \frac{1}{\sqrt{\pi}}[A_+ e^{ix_0} + A_- e^{-ix_0}]\zeta e^{-i\omega_0 t_0}. \qquad (53)$$

It might be useful here to recall that, in the case of a deep OL with an arrow gap, the macroscopic wave function for the bosons was represented as a modulation of a superposition of two Bloch modes with opposite parity, see Sec. IV. In Eq. (53) as usual, $A_+(x_2, t_2)$ and $A_-(x_2, t_2)$ are functions of slow variables independent of x_0, t_0, and $R_\perp$. The factor $\pi^{-1/2}$ before exponents is introduced for normalization. Using the ansatz (53), in the first order of ϵ ($j=1$) for the bosons we find $\omega_0 = \sigma_2(1 + M)\mathcal{K}_f\mathcal{E}_F^{3/2} + 1 + 2\nu_\perp$.

Taking into account that the expression for the fermion density ρ_1 after substituting for ψ_1 from Eq. (53) into Eq. (8) will be

$$\rho_1 = -\sigma_2\gamma|A_+ e^{ix_0} + A_- e^{-ix_0}|^2\zeta^2, \qquad (54)$$

and requiring the orthogonality of F_3 to ψ_1, we find that A_+ and A_- satisfy the following system of equations:

$$i\frac{\partial A_+}{\partial t_2} + 2i\frac{\partial A_+}{\partial x_2} - \frac{u}{2}A_- + \chi_s(|A_+|^2 + 2|A_-|^2)A_+ = 0, \quad (55)$$

$$i\frac{\partial A_-}{\partial t_2} - 2i\frac{\partial A_-}{\partial x_2} - \frac{u}{2}A_+ + \chi_s(|A_-|^2 + 2|A_+|^2)A_- = 0, \quad (56)$$

where

$$\chi_s = \frac{\nu_\perp}{\pi^2}\left(\frac{\mathcal{E}_F^{1/2}(1+M)^2|\kappa a_{bf}|^2}{2\pi M^{3/2}|\kappa a_{bb}|} - \sigma_1\right). \quad (57)$$

Equations (55) and (56) are similar to the results obtained in [25] (see also Ref. [26]) and represent the modified massive Thirring model. Using the solutions of Eqs. (55) and (56) (see [26]) in the stationary waves propagation regime, we obtain the expression of the dynamical distribution of the boson and the fermion densities in the form:

$$|\psi|^2 = \frac{\mathcal{U}\mathcal{N}_b}{2\pi}\left[\frac{1}{\sqrt{1-v^2}} + \sin(2X+\eta)\right]$$
$$\times \operatorname{sech}\left[\frac{\mathcal{U}(X-2vT)}{2\sqrt{1-v^2}}\right]\zeta^2, \quad (58)$$

$$\rho = \rho_0 - \frac{\sigma_2\gamma\mathcal{U}\mathcal{N}_b}{2\pi}\left[\frac{1}{\sqrt{1-v^2}} + \sin(2X+\eta)\right]$$
$$\times \operatorname{sech}\left[\frac{\mathcal{U}(X-2vT)}{2\sqrt{1-v^2}}\right]\zeta^2, \quad (59)$$

where $\mathcal{U} = \mathcal{U}_b - 3\sigma_2(1+M)\mathcal{K}_f\sqrt{\mathcal{E}_F}\mathcal{U}_f/2$,

$$\eta = 2\sigma_3\arctan\left\{\exp\left(\frac{\mathcal{U}}{2}\frac{X-2vT}{\sqrt{1-v^2}}\right)\right\},$$

and $\sigma_3 = \operatorname{sign}\chi_s$. It follows from Eqs. (58) and (10) that the velocity $v < 1$ is linked with the lattice parameters and the number of particles through the formula

$$\mathcal{N}_b|\chi_s| = 4\frac{1-v^2}{3-v^2}. \quad (60)$$

It can be seen from expression (58) that the bosonic component in this case always supports bright soliton solutions unlike in the case of deep lattices. At the same time, the fermion component can have dark soliton solutions when the boson-fermion interaction is repulsive ($\sigma_2 = 1$) and can have a bright soliton solution for an attractive boson-fermion interaction ($\sigma_2 = -1$). However, the effective nonlinearity of the BF mixture χ_s exerts a strong influence on the soliton amplitude: the amplitude decreases with an increase of $|\chi_s|$. Notice that in the limit when the boson-boson interaction is repulsive ($\sigma_1 = 1$) and the absolute value of the boson-fermion s-wave scattering length $|a_{bf}|$ is equal to its critical value, described by formula (28), the soliton amplitude becomes infinite. Strictly speaking this means that the method of multiple-scale expansion fails. However, it is interesting to mention that due to the normalization condition for the bosons given by Eq. (10), we have a limit on the number of bosons involved in the soliton formation and this in turn

leads to a finite amplitude for the boson density.

From the above equation, we see that for a fixed number of bosons, N_b, when $\chi_s \to 0$, $|v| \to 1$. This means that, as the soliton amplitude is increased (χ_s is decreased), the solitons are accelerated and their velocity approaches the group velocity.

VI. FERMIONS OF MODERATE DENSITY

The approximations used in the previous sections (Secs. III–V) fail when the fermionic density $\rho_0(\mathbf{r})$ vanishes at some points in space, as shown in the right column of Fig. 1. If, however, the boson-fermion interaction is much less than the interaction between the bosons, one can consider the fermionic density to be unperturbed, i.e., $\rho_1 = 0$. Then the fermionic component will contribute to the effective potential and the nonlinearity for the bosons, and the dynamics of the system will be reduced to the evolution of a bosonic component. In the present section we concentrate on this case, i.e., we assume that $\mathcal{E}_F \lesssim \mathcal{U}_f$ and require $\mathcal{E}_2 \ll \mathcal{E}_1$. This means $|a_{bf}| \ll |a_{bb}|$. The Gross-Pitaevskii equation for the macroscopic wave function for the bosons (7) is still valid and can be rewritten in the form

$$i\frac{\partial\psi}{\partial T} + \Delta_{\mathbf{R}}\psi - \nu_b^2 R_\perp^2\psi - \mathcal{U}_{eff}(X)\psi - 2\sigma_1|\psi|^2\psi = 0, \quad (61)$$

where the effective potential for the bosons, which consists of two parts [hereafter $\rho(X)$ stands for $\rho(\mathbf{R})$ at $\mathbf{R} = (X, 0, 0)$], is

$$\mathcal{U}_{eff}(X) = \mathcal{U}_b\cos(2X) + \sigma_2(1+M)\mathcal{K}_f\rho_0(X). \quad (62)$$

The first term is the OL potential and the second term is the additional potential which appears due to the boson-fermion interaction and is described by formula (A5) in Appendix A. In Eq. (62) for the effective potential, we have also taken into account that the dependence of ρ_0 on the transverse coordinate $R_\perp$ can be neglected (see the discussion in Sec. III).

The equation for the effective potential, (62), demonstrates that, even when their density is moderate, fermions can exert strong influence on the boson spectrum, as illustrated in Fig. 4. More specifically, Figs. 4(a) and 4(b) show the situation when the OL potential for the bosons ($\mathcal{U}_b$) is large. When the boson-fermion interaction is repulsive ($\sigma_2 = 1$), the effective OL for bosons becomes shallower [Fig. 4(a)] when compared with the case when fermions are absent ($\sigma_2 = 0$). This, in turn, leads to a decrease in the values of the OL band gaps [see Fig. 4(b)]. When the boson-fermion interaction is attractive ($\sigma_2 = -1$), the effective OL for bosons becomes deeper (in comparison with the case when $\sigma_2 = 0$) and the effective OL band gaps become wider. The opposite limit, when the OL potential for the bosons, $\mathcal{U}_b$, is small, is shown in Figs. 4(c) and 4(d). Even though the general effect of a decrease (increase) of effective potential for $\sigma_2 = 1$ ($\sigma_2 = -1$) is still valid as shown in Fig. 4(c), in the case of a repulsive boson-fermion interaction ($\sigma_2 = 1$), the effective potential for the bosons displays a dramatic difference in comparison to the OL potential. More specifically now one observes two minima per period (see the potential depicted by
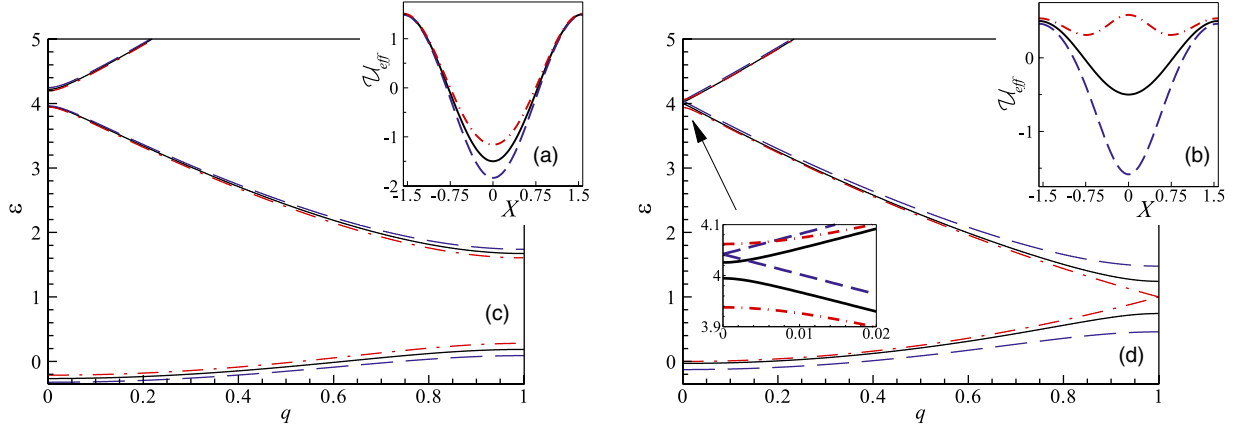
FIG. 4. (Color online) The effective potentials for the bosons (panels a,c) and the bosonic band structure (reduced zones) for the two lowest energy bands (panels b,d) when the boson-fermion interactions are absent (solid black curves), are repulsive (dash-and-dot red curves), and attractive (dashed blue curves) for the case where $a_f=(M)^{1/4}a=3.5d$, $|a_{bf}|=0.012d$, $N_f=10^4$ per period, $\mathcal{U}_f=-6.0$ and $\mathcal{U}_b=-1.5$, $M=4.0$ (panels a,b) or $\mathcal{U}_b=-0.5$, $M=12.0$ (panels c,d). The choice of these parameters is determined by the fact that we require $|a_{bf}|\ll|a_{bb}|$ to consider the fermion density to be unperturbed and at the same time to obtain considerable influence of the boson-fermion interaction on the effective potential. Thus we have to compensate the smallness of $|a_{bf}|$ by a high enough value of the relation $M=m_b/m_f$. At the same time, we also have $\mathcal{U}_f/\mathcal{U}_b\approx M$ (such as in [27]).

dash-and-dot lines in Fig. 4(c). This is due to the fact that the potential is not "monochromatic" anymore, as it is shown by the first terms of its Fourier expansion: $\mathcal{U}_{eff}(X)\approx0.435+0.008\cos(2X)+0.124\cos(4X)$. Here, the second spatial harmonic, $\cos(4X)$, is dominant. This in turn profoundly changes the band structure of the bosonic spectrum since in the absence of the second harmonic $\cos(2X)$ the Brillouin zone increases becoming $[-2,2]$ and the gap at $q=\pm1$ disappears. Now the first harmonic can be considered as a perturbation of the periodic potential having a period twice as large as the period of the original OL. As an example, one can see from Fig. 4(d), that, in the case $\sigma_2=1$, the second band gap (which is located in the vicinity of $\varepsilon=4$) is wider than the first band gap (located in the vicinity of $\varepsilon=1$), contrary to the case where boson-fermion interactions are absent, i.e., when $\sigma_2=0$.

In the case at hand, bosons just "feel" the change in the effective periodic potential due to the presence of the fermions. Thus, in the case of moderate fermion density, the boson system can be reduced to either a narrow band gap case (when $\sigma_2=1$) or to a large band gap case (when $\sigma_2=-1$). The form of a bosonic soliton is determined either by Eq. (25) (in the case of a large gap) or by Eq. (45) (in the case of a narrow gap), with the only difference that now $\gamma=0$ and $\phi_n(x_0)$ are the eigenfunctions of the operator $\mathcal{L}_x=-\partial^2/\partial x_0^2+\mathcal{U}_{eff}(x_0)$.

VII. CONCLUSION

In the present paper we have considered the formation of matter-wave solitons in a Bose-Fermi mixture embedded in a one-dimensional optical lattice and confined by a radially symmetric cigar-shaped parabolic trap. We have focused on the mean-field regime, i.e., supposed that each cell of the lattice contains a large enough number of atoms, and inves-

tigated the case wherein the number of fermions significantly exceeds the number of bosons. In such a situation, the mixture is described by the Gross-Pitaevskii equation for the bosons and by the hydrodynamic equation for the fermions, nonlinearly coupled with each other. The fermions in our study are considered spin-polarized, and thus noninteracting, and therefore the nonlinearity of the system is due to the two-body boson-boson and boson-fermion interactions. We have shown that, in spite of the essentially three-dimensional character of the fermion distribution, the evolution equation governing the dynamics of the coupled boson-fermion excitations can be effectively one-dimensional. The elements responsible for this conclusion are the strong confinement in the transverse direction and the fact that a small number of bosons occupies the lowest transverse level. We have also found that the boson-fermion interactions result in effective attractive interactions among the bosons themselves. This finding agrees with previous studies, can lead to modulational instability, and could be used for soliton generation.

We have furthermore shown that the dynamics of small-amplitude solitons is described by the nonlinear Schrödinger equation with an effective mass, in analogy to the standard situation of pure bosonic condensates loaded in an optical lattice. An essential difference in the present mixture case, in addition to the significant change of the nonlinearity, is that the effective lattice potential is originated by the optical lattice and by unperturbed spatial distribution of the fermions. This difference stems from the existence of the fermionic component in the mixture and has two immediate important consequences. First, the resulting periodic potential may be nonmonochromatic with properties different from those of the optical lattice. Second, since the longitudinal distribution of the fermions is highly sensitive to any change in the transverse configuration of the trap, a new possibility to manipulate the solitons appears. This possibility hinges on the (sometimes relatively weak) change of the transverse para-

TABLE II. Summary of the linear atomic densities for bosons and fermions obtained for different parameters of the optical lattice for bosons. In the boxes below the analytical expressions of the solitons, we indicate their type, as well as the respective formula in the text. Bright solitons of the fermionic component are understood as a local increase of the fermionic density against a background. For detailed discussion and notations see the text.

Lattice	Gap	Distribution of bosons $|\psi|^2$	Distribution of fermions ρ
Moderate $U_b \sim E_r$	Large $\Delta E \sim E_{1,2}$	$\frac{A_b}{\cosh^2(X/\ell_{bs})}|\phi_n(X)|^2$ Bright soliton; Eq. (29)	$\rho_0 - \frac{\sigma_2 A_f}{\cosh^2(X/\ell_{bs})|\phi_n(X)|^2}$ Bright (dark) soliton for $\sigma_2 < 0$ $(\sigma_2 > 0)$; Eq. (30)
		$A_b \tanh^2\left(\frac{X}{\ell_{ds}}\right)|\phi_n(X)|^2$ Dark soliton; Eq. (33)	$\rho_0 - \sigma_2 A_f \tanh^2\left(\frac{X}{\ell_{bs}}\right)|\phi_n(X)|^2$ Bright (dark) soliton for $\sigma_2 > 0$ $(\sigma_2 < 0)$; Eq. (34)
	Narrow $\Delta E \ll E_{1,2}$	$\frac{A_b}{4\cosh^2(X-vT/2\ell_{bs})}[|\phi_2(X)|^2 + |\phi_3(X)|^2]$ Bright soliton; Eq. (47)	$\rho_0 - \frac{\sigma_2 A_f}{\cosh^2[(X-vT)/2\ell_{ds}]}[|\phi_2(X)|^2 + |\phi_3(X)|^2]$ Bright (dark) soliton for $\sigma_2 < 0$ $(\sigma_2 > 0)$; Eq. (48)
		$\frac{A_b}{2}\tanh^2\left(\frac{X-vT}{\sqrt{2}\ell_{ds}}\right)[|\phi_2(X)|^2 + |\phi_3(X)|^2]$ Dark soliton; Eq. (49)	$\rho_0 - \frac{\sigma_2}{2}A_f \tanh^2\left(\frac{X-vT}{\sqrt{2}\ell_{bs}}\right)[|\phi_2(X)|^2 + |\phi_3(X)|^2]$ Bright (dark) soliton for $\sigma_2 > 0$ $(\sigma_2 < 0)$; Eq. (50)
Shallow $U_b \ll E_r$	Narrow $\Delta E \ll E_{1,2}$	$\frac{\mathcal{U}N_b}{2\pi}\frac{[(1/\sqrt{1-v^2})+\sin(2X+\eta)]}{\cosh(\mathcal{U}(X-2vT)/2\sqrt{1-v^2})}$ Bright soliton; Eq. (58)	$\rho_0 - \frac{\sigma_2\gamma N_b\mathcal{U}}{2\pi}\frac{[(1/\sqrt{1-v^2})+\sin(2X+\eta)]}{\cosh(\mathcal{U}(X-2vT)/2\sqrt{1-v^2})}$ Bright (dark) soliton for $\sigma_2 < 0$ $(\sigma_2 > 0)$; Eq. (59)

bolic trap. Moreover, since the modulational instability is usually considered as a method of generation of solitons, one can envisage the generation of solitons by means of the change of the transverse parabolic trap. This was addressed in Ref. [9] in the case of Bose-Fermi mixtures when a relatively small number of fermions are embedded in a bosonic component consisting of a much larger number of atoms. However, in this paper, we consider the situation where the number of fermions is larger than the number of bosons. Thus the effect of changing the transverse geometry is enhanced because the fermions generate an effective lattice for the bosons and thus even a very small change of the transverse distribution may have a more dramatic effect on the existence of the soliton.

We have obtained explicit expressions for gap solitons and coupled gap solitons in the case of large fermion densities and moderate boson lattices. We have also shown that bright and dark soliton solutions are possible for both the boson and the fermion components depending upon the sign of interactions and the effective mass. (For the fermionic component under the bright soliton we understand the local increase of the density against an unperturbed distribution, often well-described by the Thomas-Fermi approximation.) In the case of shallow lattices for bosons we have shown that the bosonic component always supports bright soliton solutions and the fermion component can have bright and dark soliton solutions depending on the boson-fermion interaction. For the sake of convenience, the soliton solutions obtained for the different cases considered in this paper are summarized in Table II.

We thus conclude that one has a large diversity of matter solitons even when OL is deep enough, i.e., of the order of a few recoil energies: the fermionic component can make the effective potential shallow or contribute to shrinking some of the gaps. Each of these cases requires modification of the asymptotic expansion needed for the description of the solitons and thus originates solitons with different properties. To the best of our knowledge, the respective solitons in pure bosonic condensates (where the potential is created, say, ei-

ther by low-intensity laser beams or by a superposition of laser beams of different frequencies) have not been considered in the literature, so far. The respective results, however, can be easily obtained from those presented in this paper by imposing the scattering length of boson-fermion interactions to be zero.

In all the cases considered in the present paper, the fermionic component was considered in the metallic phase. This was justified by a large number of fermions and by the transverse confinement making the distance between the transverse energy levels to be less than widths of the energy bands. This naturally means that the present research does not exhaust relevant experimentally feasible possibilities even in the regime of the mean-field approximation. In particular, we did not consider the cases of deep optical lattices, where the allowed bands are very narrow, the fermionic component is in the insulator phase, and the bosonic component is localized on a very few lattice periods giving rise to the intrinsic localized modes (or breathers).

APPENDIX A: DIRECT COMPUTATION OF THE UNPERTURBED DISTRIBUTION OF FERMIONS

To find the unperturbed density distribution of the spin-polarized fermions, we use the following approximations: (i) the fermions are spin-polarized and thus noninteracting and (ii) the trap is long enough in the direction of the optical lattice, thus allowing us to neglect boundary effects, or in other words to consider the spacial ratio $\lambda_f = 0$ in Eq. (4) and

substitute zero boundary conditions at infinity by the periodic boundary conditions. Then the single-particle wave function $\varphi_{\mathbf{q},\mathbf{m}}(\mathbf{r})$ solves the Schrödinger equation:

$$-\frac{\hbar^2}{2m_f}\Delta\varphi_{\mathbf{q},\mathbf{m}} + \frac{m_f}{2}\omega^2 r_\perp^2 \varphi_{\mathbf{q},\mathbf{m}} = E_{\mathbf{q},\mathbf{m}}\varphi_{\mathbf{q},\mathbf{m}}, \qquad \text{(A1)}$$

and thus can be represented in the form

$$\varphi_{\mathbf{q},\mathbf{m}} = e^{-r_\perp^2/2a_f^2}\frac{H_{m_y}\left(\dfrac{y}{a_f}\right)H_{m_z}\left(\dfrac{z}{a_f}\right)}{a_f\sqrt{2^{m_y+m_z}m_y!\,m_z!\,\pi}}\sum_{p=-\infty}^{\infty}c_p(q)e^{iqx+2ip\kappa x}, \qquad \text{(A2)}$$

where $\mathbf{m}=(m_y,m_z)$ are the transverse quantum numbers, $\mathbf{q}=(q,\alpha)$ where q and α are the wave vector in the first BZ and the number of the zone, respectively, $a_f=(\hbar/m_f\omega_f)^{1/2}$ is the transverse linear oscillator length of the fermionic component; $H_m(\cdot)$ are the Hermit polynomials, and κ is related to the lattice constant d as defined in Sec. II of the text. The corresponding energy eigenvalues are given by $E_{\mathbf{q},\mathbf{m}}=E_x(q)+\hbar\omega_f(m_y+m_z+1)$. The coefficients $c_p(q)$ and $E_x(q)$ can be obtained as the eigenvalues of the matrix

$$H_{p,p'} = \frac{\hbar^2(q+2p\kappa)^2}{2m_f}\delta_{p,p'} + \frac{U_f}{2}(\delta_{p,p'+1}+\delta_{p,p'-1})$$

i.e.,

$$\sum_{p'}(H_{p,p'}-\delta_{pp'}E_x)c_{p'}(q) = 0. \qquad \text{(A3)}$$

The Fermi radius can be found, supposing, that in the phase space the number of fermions per one-dimensional shell $dxdq$ is equal to $dn=dxdq/(2\pi)$. Assuming that the number of fermions N_f is large, we represent the equation for the Fermi energy in the form

$$N_f = \frac{1}{2\pi}\sum_{s=0}^{s_{max}}(s+1)\int_{-g_s}^{g_s}dq\int_{-d/2}^{d/2}dx = \frac{1}{\kappa}\sum_{s=0}^{s_{max}}(s+1)g_s,$$

where g_s are determined from the equation $E_F=\hbar\omega_f(s+1)+E_x(g_s)$, $s_{max}=[E_F/\hbar\omega_f]-1$ (here the square brackets stand for the integer value) is the number of the highest filled energy level of transverse quantization, the factor $s+1$ appears due to the transverse quantization level degeneracy.

Similarly, to find the spatial distribution of the fermion density we integrate the absolute value of the square of the wave functions (A2) over all occupied states:

$$n(\mathbf{r})\frac{\exp\left(-\dfrac{r_\perp^2}{a_f^2}\right)}{\pi^2 a_f^2}\sum_{s=0}^{s_{max}}\sum_{t=0}^{s}\frac{H_t^2\left(\dfrac{y}{a_f}\right)H_{s-t}^2\left(\dfrac{z}{a_f}\right)}{2^s t!\,(s-t)!}$$

$$\times\int_0^{g_s}\left|\sum_{p=-\infty}^{\infty}c_p(q)e^{i2p\kappa x}\right|^2 dq. \qquad \text{(A4)}$$

At $y=z=0$ the formula (A4) can be rewritten as

$$n(x,0,0) = \frac{1}{\pi^2 a_f^2}\sum_{s=0}^{[s_{max}/2]}\sum_{t=0}^{s}\frac{(-1)^s}{2^s(2t)!\,!\,(2s-2t)!\,!}$$

$$\times\int_0^{g_{2s}}\left|\sum_{p=-\infty}^{\infty}c_p(q)e^{i2p\kappa x}\right|^2 dq. \qquad \text{(A5)}$$

Notice that if

$$\int_{-d/2}^{d/2}\left|\sum_p c_p(q)e^{i2p\kappa x}\right|^2 dx = d \qquad \text{(A6)}$$

[or, equivalently, $\Sigma_p|c_p(q)|^2=1$], the normalization condition

$$\int d\mathbf{r}_\perp\int_{-d/2}^{d/2}dx\,n(\mathbf{r}) = \frac{1}{\kappa}\sum_{s=0}^{s_{max}}(s+1)g_s = N_f$$

is met.

APPENDIX B: ON THE MULTIPLE SCALE EXPANSION

For the sake of completeness here we present some details of the multiple-scale expansion used throughout the text.

The first three functions F_j ($j=1,2,\dots$) in the right-hand side of Eq. (15) are given by $F_1=0$,

$$F_2 = -i\frac{\partial\psi_1}{\partial t_1} - 2\frac{\partial^2\psi_1}{\partial x_0\,\partial x_1},$$

$$F_3 = -i\frac{\partial\psi_1}{\partial t_2} - 2\frac{\partial^2\psi_1}{\partial x_0\,\partial x_2} - \frac{\partial^2\psi_1}{\partial x_1^2} - i\frac{\partial\psi_2}{\partial t_1} - 2\frac{\partial^2\psi_2}{\partial x_0\,\partial x_1}$$

$$+ 2\sigma_1|\psi_1|^2\psi_1 + \sigma_2(1+M)\mathcal{K}_f\rho_1\psi_1$$

where $j=1,2,\dots$ coincides with the order of ϵ at which the equation is obtained.

Next we define the eigenfunctions $\phi_{n,q}(x)$ of the operator $\mathcal{L}_x$: $\mathcal{L}_x\phi_{n,q}(x_0)=\varepsilon_{n,q}\phi_{n,q}(x_0)$, where n and q refer to the band number and to the wave vector in the first Brillouin zone. For the Bloch functions bordering an edge of the Brillouin zone, i.e., for $q=\pm1$, we introduce the notation $\phi_n(x)\equiv\phi_{n,\pm1}(x)$. These functions are real. Next we consider the eigenvalue problem for the 2D harmonic oscillator $\mathcal{L}_\perp\zeta_{lm}(\mathbf{R}_\perp)=[2(l+m+1)\nu_\perp]\zeta_{lm}(\mathbf{R}_\perp)$ and for its ground state we introduce the notation $(R_\perp=|\mathbf{R}_\perp|)$

$$\zeta(R_\perp)\equiv\zeta_{0,0}(\mathbf{R}_\perp) = \left(\frac{\nu_\perp}{\pi}\right)^{1/2}e^{-1/2\nu_\perp R_\perp^2}. \qquad \text{(B1)}$$

[1] V. A. Brazhnyi and V. V. Konotop, Mod. Phys. Lett. B **18**, 627 (2004).

[2] O. Morsch and M. Oberthaler, Rev. Mod. Phys. **78**, 179 (2006).

[3] V. V. Konotop and M. Salerno, Phys. Rev. A **65**, 021602(R) (2002).

[4] H. Pu, L. O. Baksmaty, W. Zhang, N. P. Bigelow, and P. Meystre, Phys. Rev. A **67**, 043605 (2003); A. V. Yulin, D. V. Skryabin, and P. S. J. Russel, Phys. Rev. Lett. **91**, 260402 (2003); H. Sakaguchi and B. A. Malomed, J. Phys. B **37**, 1443 (2004); B. J. Dabrowska, E. A. Ostrovskaya, and Yu. S. Kivshar, J. Opt. B: Quantum Semiclassical Opt. **6**, 423 (2004).

[5] L. Pezzè, L. Pitaevskii, A. Smerzi, S. Stringari, G. Modugno, E. DeMirandes, F. Ferlaino, H. Ott, G. Roati, and M. Inguscio, Phys. Rev. Lett. **93**, 120401 (2004).

[6] G. Mundugno, G. Roati, F. Riboli, F. Ferlaino, R. J. Brecha, and M. Iguscio, Science **297**, 2240 (2002).

[7] F. Schreck, G. Ferrari, K. L. Corwin, J. Cubizolles, L. Khaykovich, M.-O. Mewes, and C. Salomon, Phys. Rev. A **64**, 011402(R) (2001).

[8] R. Roth, Phys. Rev. A **66**, 013614 (2002).

[9] T. Karpiuk, M. Brewczyk, S. Ospelkaus-Schwarzer, K. Bongs, M. Gajda, and K. Rzazewski, Phys. Rev. Lett. **93**, 100401 (2004).

[10] J. Santhanam, V. M. Kenkre, and V. V. Konotop, Phys. Rev. A **73**, 013612 (2006).

[11] T. Karpiuk, M. Brewczyk, and K. Rzazewski, Phys. Rev. A **69**, 043603 (2004).

[12] T. Tsurumi and M. Wadati, J. Phys. Soc. Jpn. **69**, 97 (2000).

[13] G. M. Bruun and C. W. Clark, Phys. Rev. Lett. **83**, 5415 (1999).

[14] M. Salerno, Phys. Rev. A **72**, 063602 (2005).

[15] M. Centelles, M. Guilleumas, M. Barranco, R. Mayol, and M. Pi, Laser Phys. **16**, 360 (2006).

[16] F. Ferlaino, C. D'Errico, G. Roati, M. Zaccanti, M. Inguscio, G. Modugno, and A. Simoni, Phys. Rev. A **73**, 040702(R) (2006).

[17] K. Mølmer, Phys. Rev. Lett. **80**, 1804 (1998).

[18] M. A. Morrison, T. L. Estle, and N. F. Lane, *Quantum States of Atoms, Molecules, and Solids* (Prentice-Hall, Englewood Cliffs, NJ, 1976).

[19] J. Kevorkian and J. D. Cole, *Multiple Scale and Singular Perturbation Methods* (Springer, New York, 1996), Chap. 6.

[20] H. Pu, L. O. Baksmaty, W. Zhang, N. P. Bigelow, and P. Meystre, Phys. Rev. A **67**, 043605 (2003).

[21] N. W. Ashcroft and N. D. Mermin, *Solid State Physics* (Saunders College Publishing, Fort Worth, TX, 1976).

[22] V. V. Konotop and G. P. Tsironis, Phys. Rev. E **53**, 5393 (1996).

[23] V. V. Konotop, Phys. Rev. E **53**, 2843 (1996); S. Jiménez and V. V. Konotop, Phys. Rev. B **60**, 6465 (1999).

[24] This phenomenon was observed in numerical studies of wave propagation in photonic crystals by J. Peyraud and J. Coste, Phys. Rev. B **40**, 12201 (1989).

[25] A. B. Aceves and S. Wabnitz, Phys. Lett. A **141**, 37 (1989).

[26] A. I. Maimistov and A. M. Basharov, *Nonlinear Optical Waves* (Kluwer Academic Publishers, Dordrecht, The Netherlands, 1999).

[27] G. Modugno, F. Ferlaino, R. Heidemann, G. Roati, and M. Inguscio, Phys. Rev. A **68**, 011601(R) (2003).